Rayleigh-linewidth measurements on thin critical fluid films

Stephen A. Casalnuovo,* R. C. Mockler, and W. J. O'Sullivan
Department of Physics, University of Colorado, Boulder, Colorado 80309
(Received 15 August 1983)

We describe photon autocorrelation measurements of the Rayleigh linewidth in thin binary liquid films near the critical point. Measurements were made on four films of thickness 13.1, 4.1, 2.1, and 0.5 μm. The films were formed by trapping and sealing samples of a 2,6-lutidine + water critical mixture between fused-silica optical flats. Dynamic scaling arguments predict that the Rayleigh linewidth dependence upon $k\xi$ for the films should be indistinguishable from that for otherwise identical large-volume samples, until conditions defined by both $\xi \simeq s/2$ and $\Lambda \simeq s$ are satisfied. Here, s is the film thickness, ξ is the correlation length, and $\Lambda \equiv 2\pi k^{-1}$ is the sampling length probed at wave number k. We find that, for the three thicker films to within 0.1 mK of their phase-separation temperatures and for the 0.5-μm film to within 2 mK of an extrapolated critical temperature, our data agree with the predictions of renormalization-group theory for binary liquid mixtures in three spatial dimensions—with no adjustable parameters. No evidence of finite-size effects was seen, although both conditions are at least marginally satisfied for the 0.5-μm film ($\Lambda \simeq s$, and eight linewidths measured with $\xi > s/2$) and for the 2.1-μm film ($\Lambda \simeq s/4$, and fourteen linewidths measured with $\xi > s/2$). No effects were seen that could be traced to the presence of surface wetting layers. Finally, we observe a time- and film-thickness-dependent drift in the critical temperature which is not a critical phenomenon, and we find evidence for a noncritical phase transition in the thinnest film.

I. INTRODUCTION

The key experimental quantity used to compare the dynamic critical properties of classical liquids with theory is the Rayleigh linewidth of light scattered by order-parameter fluctuations, measured near the critical point as a function of fluctuation wave number k and temperature. In Rayleigh linewidth studies on critical liquids, typical sample linear dimensions are about 1 cm. There are two important lengths which are central to an understanding of these experimental results, the correlation length ξ of the order-parameter fluctuations and the characteristic *sampling length* Λ defined by $\Lambda = 2\pi(k)^{-1}$. Since typical Λ values and the practical upper limit on ξ are roughly 1 μm, these conventional Rayleigh linewidth experiments probe the dynamic response of critical fluids in the large-volume limit where effects due to specific surface boundary conditions are generally irrelevant.

During the last decade, precise Rayleigh linewidth data have been collected for a number of binary liquid critical mixtures,[1] with the recent work by Burstyn, Sengers, and co-workers[2–5] on 3-methylpentane+nitroethane serving as a definition of the best of this class of experiment. The excellent agreement between these data and the predictions of mode-mode coupling,[6,7] and dynamic renormalization group[8] (RG) theories leave little doubt that these models provide a fundamentally correct representation of classical liquid critical dynamics in three dimensions (3D). While legitimate questions of detail remain to be examined, it is probably safe to associate the cliche *well understood* to the dynamic critical behavior of classical liquids in the large-volume limit.

In principle, liquid critical behavior can be examined under conditions that reveal the influence of restricted geometry and surface boundary effects, if we change the conventional sample configuration in either of two ways. Consider a bulk sample of a binary liquid at the critical composition and confined within a cube of volume L^3. Imagine inserting a flat boundary wall of cross section $A < L^2$ into the cube, parallel to one of its faces and separated from it by a distance $s \ll L$. The fluid between the inserted boundary and the cube face forms a film of thickness s. Since $A < L^2$, the fluid comprising the film is in thermodynamic contact with a surrounding reservoir of bulk fluid with which it can exchange material. This is an *open* film. In contrast, imagine inserting a square boundary of area L^2 in the same way as above so that the fluid forming the film is sealed and isolated from the remainder of the sample. If this process is carried out very quickly, the trapped film will be formed at the bulk sample critical composition. We will refer to the final result as a *closed* film.

Fisher and co-workers[9–12] have considered the static critical properties of open films. In this case a rich assortment of phenomena are predicted, associated with the growth of critical surface layers as well as with finite-size effects due to the suppression of critical fluctuations when $\xi \geq s/2$. However, open binary liquid films present difficulties to the experimentalist. In general, one of the liquid components will have a greater surface tension relative to the solid surfaces that confine the film. Since the system will be in a lower energy state when that component accumulates at the surface, material is exchanged between film and reservoir leading to the formation of surface wetting

layers.[13] Significant composition gradients will form, and eventually the film will be pulled from the critical composition. These effects are particularly important for thin films ($s < 1$ μm), where surface layers can account for a large fraction of the total film volume, and where the approach to an eventual equilibrium configuration may take days to complete near a critical point.[14]

Although a closed critical binary liquid film is a nontrivial thermodynamic system, elimination of material exchange between film and reservoir ensures that the film composition is at least globally stable over time, and should lead to a suppression of surface layer growth. There has been no theoretical study of the static critical properties of closed films comparable to that carried out on open films. We know of no published theoretical work which treats the dynamic critical behavior of either class of liquid film.

In this paper we report details of the first Rayleigh linewidth measurements on thin critical liquid films. Closed films of the binary mixture 2,6-lutidine+water were formed at the large-volume critical composition, and at thicknesses s of 13.1, 4.1, 2.1, and 0.5 μm. Measurements on the 2.1-μm film extended into the correlation-length regime defined by $\xi \geq s/2$, and in the case of the 0.5-μm film into the regime defined by $\xi \geq s/2$ and $\Lambda \simeq s$. A brief report of the results on the three thickest films was published earlier.[15]

The emphasis in this paper is placed on the experiment and the experimental results, which are treated in Secs. III and IV, respectively. Section II A includes a brief discussion of some modifications of liquid dynamic critical behavior that might occur in thin closed films, and in Sec. II B we discuss changes in the light scattering formalism which occur in films. Section V consists of a brief final summary.

II. CRITICAL FLUID FILMS: IMPLICATIONS FOR THE RAYLEIGH LINEWIDTH AND LIGHT SCATTERING

A. The Rayleigh linewidth

In this section we discuss possible effects on the Rayleigh linewidth of confining a binary-liquid critical mixture in a closed thin film. We consider finite-size effects from the perspective of the scaling hypothesis, the relation between boundary conditions and the film dynamic universality class, and finally, the possible effects due to the formation of surface wetting layers.[13] Since no proper theoretical study of critical dynamics in thin fluid films has been carried out, our discussion is conjectural.

The RG prediction for the Rayleigh linewidth[8] in the infinite-volume limit is

$$\Gamma = [Rk_B T/6\pi\eta(\xi)\xi^{d-2}]k^2\Omega(k\xi) \quad (1)$$

where R is a universal amplitude ratio, $d=3$, the number of spatial dimensions, and $\Omega(k\xi)$ is a universal scaling function. In the extreme hydrodynamic limit,

$$\Gamma = A\xi^{2-z}k^2 , \quad k\xi \ll 1 \quad (2)$$

and for fixed k, as $\xi \to \infty$, the linewidth behaves as

$$\Gamma = Bk^z , \quad k\xi \gg 1 \quad (3)$$

where z is the dynamic critical exponent with the value $z=3.065$ for $d=3$ and for the binary liquid universality class[16] (model H of Ref. 16); A and B are constants. The $\xi \to \infty$ limiting behavior can be understood from scaling theory[17] to reflect the requirement that ξ should be replaced by k^{-1} when the correlation length exceeds k^{-1}. That is, ξ becomes irrelevant when $\xi > k^{-1}$.

In the hydrodynamic regime ($k\xi \ll 1$) the surface boundary conditions are unimportant and the film Rayleigh linewidths should be identical to those measured in large samples having the same composition and at identical values of $k\xi$. As the critical point is approached more closely, ξ increases until $\xi \simeq s/2$, and further growth of the order-parameter fluctuations is constrained to the plane of the film. This defines the condition under which finite-size modifications of the *static* critical properties of fluid films should occur, identified by a 3D-to-2D Ising class transformation. Fisher[9] has discussed finite-size effects of this type.

Similarly, in the dynamic case,[18] the scaling form for the order-parameter relaxation rate in 3D,

$$\omega_\psi(k) = k^{3.065}\Omega(k\xi) , \quad (4)$$

will reflect the film response as long as the sampling wavelength Λ is significantly shorter than the film thickness s, even in the limit $\xi \to \infty$. Thus, an ingenuous application of scaling considerations to thin critical films leads to the conclusion that, until the conditions $\Lambda \geq s$ and $\xi \geq s/2$ are simultaneously satisfied, the film Rayleigh linewidth will be identical to that measured in a conventional sample at the same value of $k\xi$.

When both finite-size conditions are satisfied, we presume that a crossover should occur in the dynamic universality class, reflecting the relevance of the boundary conditions, and in the spatial dimension, from $d=3$ to $d=2$.

We emphasize that these conclusions are problematic. This unsophisticated application of scaling arguments to thin critical film dynamics ignores complications associated with the formation of substantial surface wetting layers. The boundary conditions (vanishing of the velocity at the walls and nonconservation of the fluid momentum[19]) may have important dynamical effects when $\xi \simeq s/2$, even for sampling wavelengths smaller than the film thickness.

Related to this point, Gutkowicz-Krusin *et al.*[20] used a linearized hydrodynamic approach to analyze the influence of the thin-film geometry on density fluctuations in single-component liquids. They find that the Rayleigh linewidth is relatively unaffected by a variety of surface boundary conditions. However, their results are restricted to the $k\xi < 1$ regime. Nevertheless, since we probe the $k\xi < 1$ regime in this experiment our results should test their predictions.

Halperin[19] suggests that sufficiently close to the critical point the universality class for our closed films will shift from model H with $d=3$, in the classification scheme in-

troduced in Ref. 16, to that of a 2D Ising model with conserved order parameter and no momentum conservation, model B with $d=2$. This transformation would be noted by a change in the critical exponent z:

$$z=3.065 \text{ (model } H,\ d=3)\ ,$$

$$z=3.91 \text{ (model } B,\ d=2)\ .$$

If the scaling arguments are valid, evidence for this transformation would appear only for $\Lambda \geq s$ and $\xi \geq s/2$. These values of z are calculated using the ϵ expansion, where $\epsilon=4-d$ is assumed to be a small parameter. Although the 3D value has been verified by experiment,[2] the 2D value probably only has qualitative significance.

There is one final problem that complicates the determination of the critical dynamics of these films. The results of recent theoretical[10,12,13] and experimental[14,21–24] work argue for the existence of a surface layer due to the preferential wetting of one liquid component on the solid walls bounding the film. The thickness of this wetting layer is expected to grow as the correlation length ξ, and need not be small compared to the film thickness for temperatures near the critical point. Fisher and Nakanishi[12] have shown that the surface layers which develop in open films in the presence of two closely spaced walls will induce concentration gradients. In the simplest view, the film will be pulled off the critical composition, moving the system away from the critical point if the gradients are sufficiently large. This effective off-loading should lead to increased Rayleigh linewidths and reduced scattering intensities. In addition, because the surface layers may be particularly sensitive to the boundary conditions at the walls their dynamical response may be different than that of the fluid in the body of the film.

We can summarize this section as follows. If simple scaling arguments prevail, the film Rayleigh linewidths should be identical with those measured, under otherwise identical conditions, on a large sample, until $\Lambda \simeq s$ and $\xi \simeq s/2$. At this point a universality class transformation should occur, possibly from[16] model H, $d=3$ to model B, $d=2$. This should be detectable from measurements of the critical exponent z. The possibility exists that important dynamic effects due to the surface boundary conditions might vitiate these conclusions. A mode-coupling calculation which includes the film boundary conditions will probably have to be done in order to settle this point. Finally, the formation of surface wetting layers could complicate the interpretation of Rayleigh linewidths measured on thin-film samples.

B. Light scattering

Diffraction effects modify the angular distribution of the scattered electric field $\vec{E}(\vec{k}_{sc})$ when the film thickness becomes comparable to the wavelength of the incident light. The scattering vector has the usual definition (see Fig. 1),

$$\vec{k}_{sc} \equiv \vec{k}_0 - \vec{k}_i$$

and

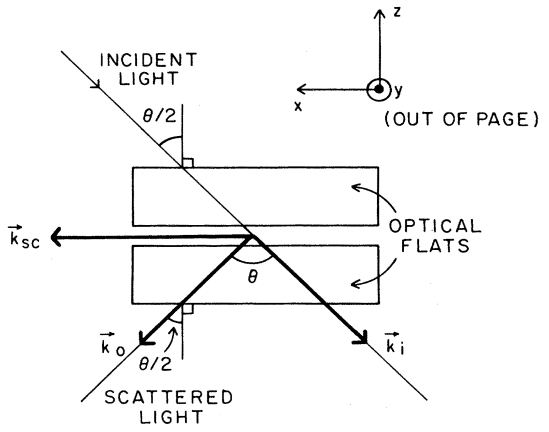

FIG. 1. Scattering geometry with $\vec{k}_{sc}$ lying in the plane of the film.

$$k_{sc}=|\vec{k}_{sc}|=\frac{4\pi}{\lambda}\sin\left[\frac{\theta}{2}\right]\ ,$$

where θ is the scattering angle and λ is the operating wavelength of the laser. Both the incident and the scattered electric field are polarized along the y direction in Figs. 1 and 2. The scattered-field angular distribution depends on the form chosen for the boundary conditions that the order-parameter fluctuations must satisfy at the walls. We have required that the component of the gradient of the concentration fluctuations normal to the plane of the film must vanish at the boundaries and have calculated the scattered field for this case.[25]

The effect of this boundary condition (normal component of the fluctuation gradient vanishes at the boundaries) is to quantize the component of the fluctuation wave vector $\vec{k}$ ($k=|\vec{k}|$) normal to the surfaces. For the scattering geometry of Fig. 1, only the zeroth-order mode contributes to the scattering and the result is the same as for the infinite-volume case,[26] namely,

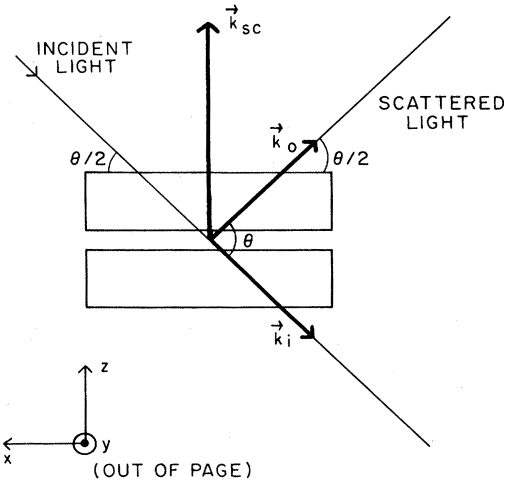

FIG. 2. Scattering geometry with $\vec{k}_{sc}$ perpendicular to the film.

$$\vec{E}(\vec{k})=\hat{\epsilon}_y A\delta(\vec{k}-\vec{k}_{sc}) , \quad (5)$$

where A is a system-specific constant, $\hat{\epsilon}_y$ is the polarization unit vector, and where the appearance of the delta function depends on the transverse dimensions of the film being very large compared to the light wavelength. This simple result can be attributed to the absence of a normal component of $\vec{k}_{sc}$ for this particular scattering geometry.

In Fig. 2 we show a scattering geometry in which $\vec{k}_{sc}$ is normal to the plane of the film. In this case we find

$$\vec{E}(\vec{k})=\hat{\epsilon}_y A \sum_{n=0}^{\infty} \sin(K_n s)/(K_n s) , \quad (6)$$

where s is the film thickness and $K_n=n\pi/s-k_{sc}$. This has maxima when $k_{sc}=n\pi/s$ or when the magnitude of the scattering vector matches one of the wave numbers of the modes selected by the boundary condition. In addition, the wave-number selection rule, Eq. (5), no longer holds. Even though the scattered field is a maximum when $\vec{k}=\vec{k}_{sc}$, a range of fluctuation wave numbers k contributes to the field scattered at a given angle due to the finite width of the function $\sin x/x$. If we take the width Δk to be the width of the central maximum then $\Delta k/k=(\pi/s)/(n\pi/s)=1/n$. For low-order modes the spread is comparable to k itself, which should have a significant effect on the measured Rayleigh linewidths. Each fluctuation wave number k contributes an exponential term of the form $\exp[-\Gamma(k)t]$ to the measured autocorrelation function of the scattered field.[27] A range of wave numbers will contribute a continuous distribution of exponential terms.

In practice, we fit our measured autocorrelation functions to an exponential whose argument is a power series in t, even when only the linear term is expected. All terms of higher order in t should be negligible for a single exponential, but the higher-order terms should become comparable to the linear term for the distribution of exponentials expected when $s\simeq\lambda$. A test of the smearing out of the wave number selection rule, then, is to watch for the increase in magnitude of the higher-order terms with decreasing film thickness.

III. EXPERIMENT

A schematic of the overall experiment is shown in Fig. 3. Vertically polarized and attenuated light from an argon-ion laser (Spectra Physics Model 165) operating in a single-frequency, multimode configuration enters the two-beam heterodyne system. Light scattered quasielastically from the film mounted in a thermostated chamber is added coherently to the local oscillator beam at a beam splitter, and then detected by a cooled International Telephone and Telegraph Co. FW130 photomultipler tube (PMT). The photocurrent is fed into a Langley-Ford 64-channel correlator which is on line to a Digital Equipment Corporation LSI-11 computer where the data are stored and analyzed.

In this section we present a summary of those details of the experiment which are germane to light scattering studies on thin critical fluid films.

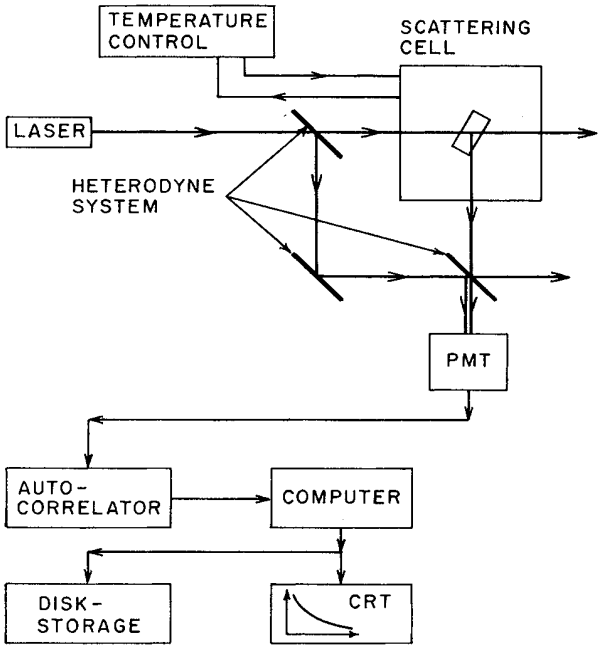

FIG. 3. Block diagram of the experiment.

A. The heterodyne spectrometer

Random surface imperfections in the fused-silica optical flats that confine the film scatter sufficient light to produce an uncontrollable heterodyne component in the autocorrelation function. Even for a film as thin as 2.1 μm, the homodyne signal and this spurious heterodyne contribution make comparable contributions to the autocorrelation function.

In order to get reproducible and unambiguous Rayleigh linewidth data from thin films the two-beam heterodyne system shown in Fig. 4 was developed. By adjusting the intensity of the local oscillator beam routed outside the thermostated chamber, the heterodyne signal can be made sufficiently strong compared to the homodyne signal so that the homodyne part can be ignored.

Mechanical stability is the crucial design consideration for this system. Relative motion between the two light paths produces a spurious contribution to the measured autocorrelation function and alters the apparent Rayleigh linewidth. Thus, all optical components are securely mounted and great care is taken to eliminate sources of vibration. The assorted beam splitters, the mirror, and the crossed polarizers are mounted on a steel plate bolted to the outer can of the thermostated chamber with the cell mounted rigidly inside. The entire apparatus is kept as small as possible to reduce motion. The optical components are glued onto optical mounts originally designed to hold end mirrors in laser cavities. These are massive brass mounts each with two degrees of high-resolution angular adjustment and exceptional pointing stability. These mounts are glued to magnetic stands that fix them to the steel plate. The angular adjustment permits the alignment of the local oscillator with the scattered light along the

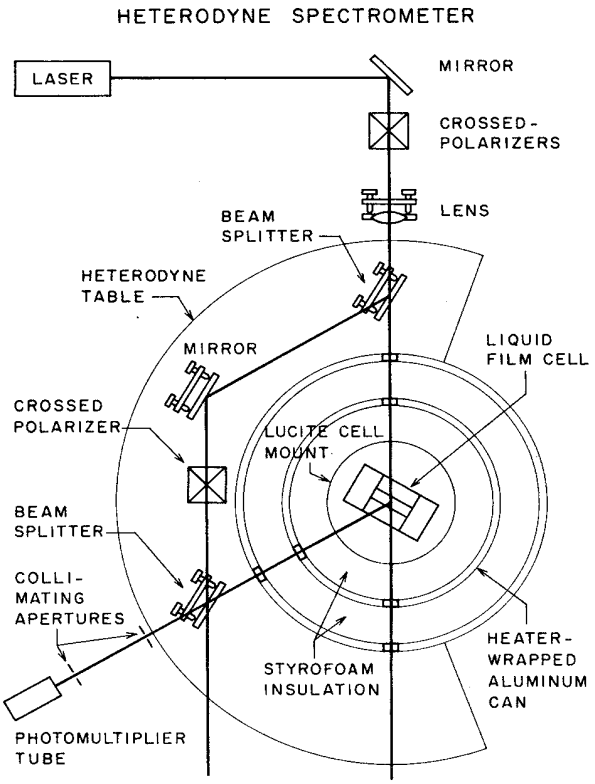

FIG. 4. The heterodyne spectrometer. Path lengths of the two arms are kept equal to within 2 cm to minimize wave-front mismatch.

optical axis of the PMT. The stability is such that the detector holds its alignment over a 24-hour period without any additional adjustment.

B. Thin-film cell

In this experiment we wish to probe the correlation-length regime defined by $\xi \geq s/2$, where ξ will be assumed to scale with temperature as $\xi = \xi_0 \mid T - T_c/T_c \mid^{-\nu}$ with $\nu = 0.63$. For 2,6-lutidine+water, $\xi_0 = 2$ Å and $T_c = 304$ K. If the sample temperature can be controlled to ± 0.1 mK, so that a minimum value of $\mid T - T_c \mid \simeq 0.1$ mK is achievable, then 5 μm represents an *upper limit* on the film thickness such that $s \simeq 2\xi$ becomes technically feasible. The requirement that we be able to probe fluctuation wavelengths that are comparable to the film thickness introduces a second, equally important design consideration. Ideally, this experiment should be carried out as a function of scattering angle, and should include small scattering angles ($\theta \leq 5°$) where the condition $\Lambda \geq s$ can be satisfied even for films as thick as 5 μm. However, when we faced the problem of experimental design, our overwhelming concern was with the basic question of technical feasibility. It was not clear that data of useful quality could be taken on thin critical fluid films with scattering volumes up to 3 orders of magnitude smaller than those used in conventional Rayleigh linewidth measurements on critical fluids.[1-5] We designed our system around a fixed scattering angle of 60°. In this case, $\Lambda \simeq \lambda$, the laser wavelength. If the argon-ion laser is operated at a wavelength of 514.5 nm, the condition that $\Lambda \geq s$ requires that $s \leq 0.5$ μm.

The cell used to form the binary liquid films is depicted schematically in Fig. 5 and redrawn in the exploded view of Fig. 6. The cell body is a stainless-steel cylinder with a diameter of 6 cm and a height of 5 cm. The films are confined between fused-silica optical flats 2.54 cm in diameter and 0.95 cm thick. Sandwiched between the flats is a ring-shaped gasket that sets the thickness of the liquid film. For films thicker than 1 μm this spacer ring is cut from gold foil of the appropriate thickness. For films thinner than 1 μm, the gold foils proved to be too fragile to handle. In this case, a ring of SiO of the desired thickness was deposited on one of the flats using photolithography equipment at the National Bureau of Standards in Boulder. The *O*-rings are Teflon encapsulated rubber *O*-rings manufactured by the A. W. Chesterton Co.

Film thicknesses were measured using a method developed by Hurd[28] for his work on thin colloidal films. A diagram is given in Fig. 7. Coherent light from a laser is incident upon the liquid film and reflected by the two glass-liquid interfaces. The phase of the light reflected from the second interface is delayed relative to that reflected by the first due to the additional optical path length through the film. When the film is thinner than roughly the width of the laser beam, which is about one millimeter, the two reflections overlap and interfere. The incident angle θ is varied between 0° and the maximum of 55° allowed by the size of the cell, and the angles at which destructive interference occurs are noted. The precision of this method is improved by locating the film within the focal length of a converging lens and by focusing the beam on a screen. A destructive interference fringe appears as the total extinction of the laser spot on the screen. With these angles, the refractive index of 2,6-lutidine+water,[29] and the laser wavelength, the film thickness can be determined to within a few tenths of a micrometer.

This procedure is useful for film thicknesses down to approximately 1 μm. Variations of it, which involve the use of several different wavelengths, extend its application to thicknesses as small as 0.1 μm.

The film spacing uniformity is determined using the

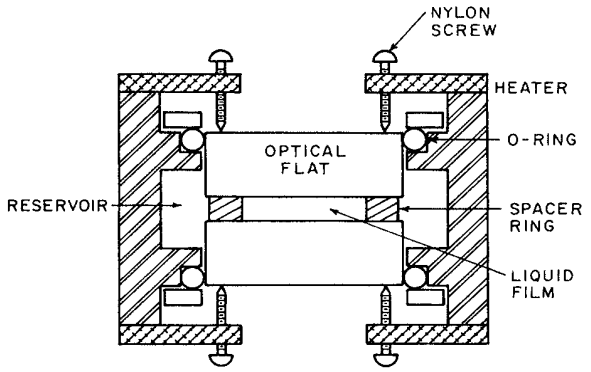

FIG. 5. The thin-film cell.

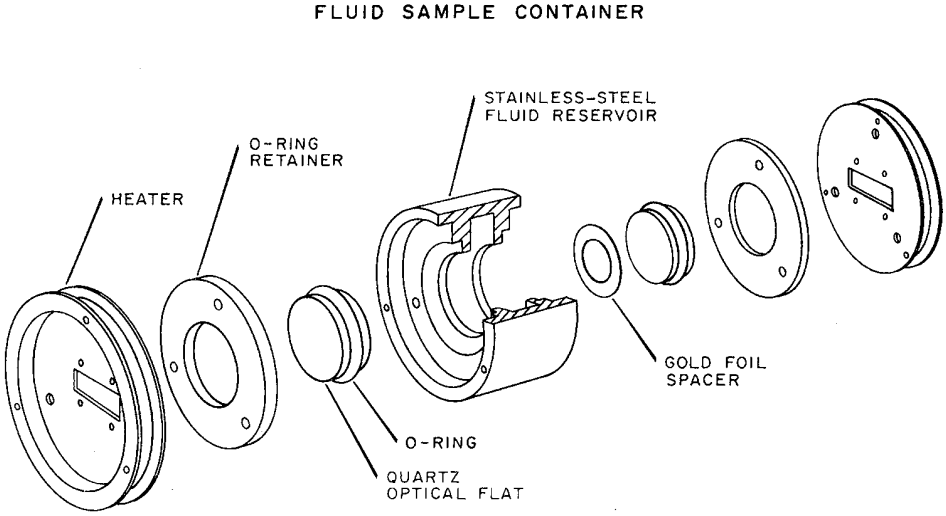

FIG. 6. An exploded view of the thin-film cell.

procedure shown in Fig. 8. A beam expander is adjusted to give a converging beam with a focal length of approximately one meter. The cell is placed within the focal length so that the beam completely spans the film and is turned at some angle to the beam. If the reflections are observed close to the cell, the more intense reflections from the two air-glass surfaces completely obscure the reflected interference pattern. At the focal point of the beam, the reflections are separated in space and the unwanted reflections can be masked off. The desired interference pattern is then observed on a screen. In this interference pattern, lines of destructive interference correspond to contours of equal thickness. If the film thickness is not sufficiently uniform the nylon screws pressing the flats together are adjusted and the spacing rechecked. This procedure produces films that are uniform to within $\pm 0.1\ \mu$m.

A technique similar to that shown in Fig. 7 is used to measure the thermal expansion and spacing stability. The cell is placed within the thermostated chamber which has windows to allow the laser beam to enter and the reflected beams to exit. The position of the windows fixes θ at 30°.

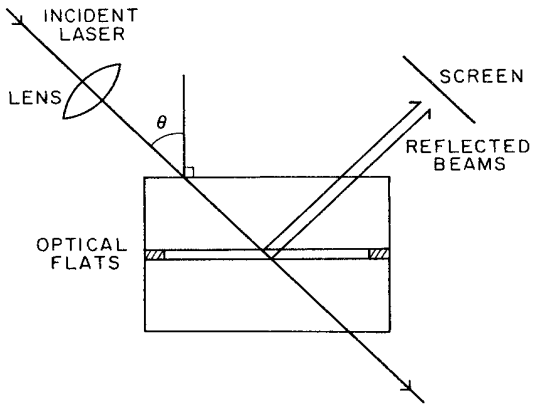

FIG. 7. The technique used to measure film thickness.

A laser power meter monitors the intensity of the interference spot and its output is recorded on a strip-chart recorder. The cell then is warmed to approximately T_c. Any change in spacing due to thermal expansion appears as a change in the intensity of the interference spot. Once the cell has come to thermal equilibrium, the spacing change can be determined by counting the number of passing fringes recorded on the strip chart. Figure 9 shows the initial expansion and the subsequent thermal equilibrium spacing stability in a 2.1-μm film and is typical of the small expansion observed. One can see that there is very little change in the cell spacing over many hours once the system has stabilized. In addition, the thickness of each film was remeasured after a complete set of data was taken, approximately one month after the film was formed. In all cases it agreed well with the film thickness measured originally.

C. Temperature control

The temperature control system, consisting of a thermostated sample chamber and temperature regulating and monitoring electronics, is similar in design and performance characteristics to that developed by Sorenson.[30] It is capable of maintaining the temperature of a liquid sample within 0.1 mK of the critical temperature with a stability of $\pm 40\ \mu$K/day.

The thermostated chamber developed for the film studies consists of three "cans" as shown in Fig. 10; an outer cylindrical aluminum can, an inner cylindrical aluminum can, and the film cell. The outer can is not temperature controlled and serves just as a rigid container for the others. It has a diameter of 22 cm, a height of 22 cm, and its walls are 1 cm thick. The inner can is 17 cm in diameter, has a height of 17 cm, and its walls are 0.7 cm thick. The cans are separated by a layer of plastic foam insulation. The thin-film cell is rigidly mounted in a Plexiglass cylinder fixed inside the inner can and insulated by another layer of plastic foam.

The temperature of the inner can is controlled using a

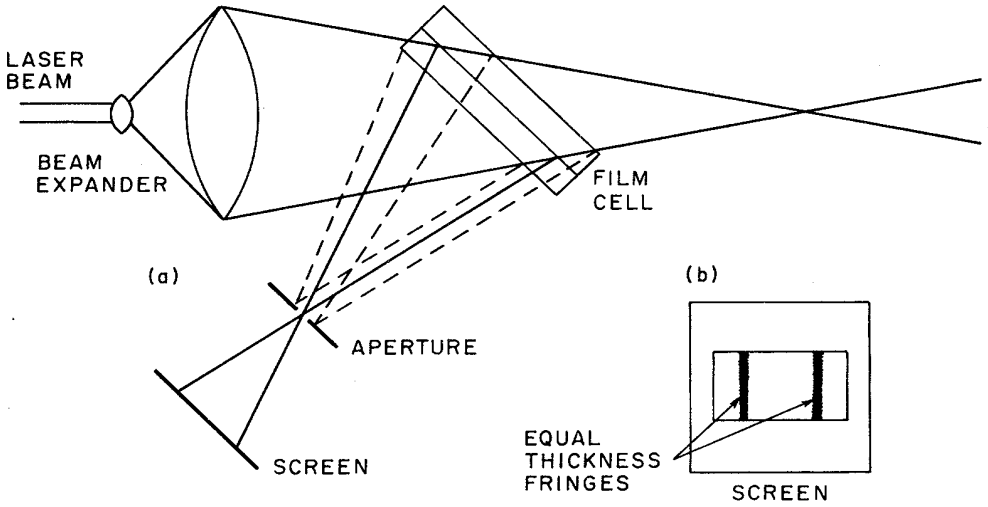

FIG. 8. The method used to assess the uniformity of the film thickness: (a) the optical arrangement; (b) an interference patterm.

dc Wheatstone bridge and rate-sensing power amplifier.[31] The temperature sensor is a Fenwall GA42P2 thermistor mounted in the can close to the heating wire to minimize the lag time of the circuit. The stability of this bridge is 0.1 mK over several hours. The sample temperature is controlled and monitored by two independent ac Kelvin double bridges, each with a Fenwall GA42P2 thermistor sensor. These bridges have temperature resolutions of 0.03 mK, limited by the requirement that thermistor self-heating be kept below 0.1 mK. The bridges are stable to within 0.05 mK over several days.

The effects of laser heating in the liquid film must also be accounted for if accurate knowledge of the temperature is desired. In their studies of the 3-methylpentane and nitroethane mixture Sorensen *et al.*[32] and Burstyn and Sengers[2] found laser heating to be about 1 mK/mW. This was measured by monitoring the change in the scattered light intensity with time as a function of laser power. It is not possible to repeat this measurement on the liquid films. Random intensity variations in the scattered light, probably due to slight displacements of the laser beam which change the scattering intensity from the fluid-flat interfaces, make relative intensity measurements unreliable. We estimate the effect of laser heating by assuming that the temperature coefficient is the same as in the 3-methylpentane and nitroethane system. In the 13.1- and 4.1-μm films, the laser power was kept at or below 0.1 mW, corresponding to a 0.1-mK warming. In the 2-μm film, the power was never greater than 0.2 mW, giving at most a 0.2-mK warming; 0.5 mW was used for the 0.5-μm film so a 0.5-mK warming could be expected. These temperature changes are not negligible compared to the resolution of the temperature measurements. The data were not corrected for the change because of the imprecision of the estimates. Since the linewidth is measured below T_c in the one-phase region, the effect of the laser heating is to push the system close to T_c and toward larger values of the correlation length. Therefore, if any finite-size effects are present in the Rayleigh linewidth data when $\xi > s/2$ they will not be obscured by laser heating.

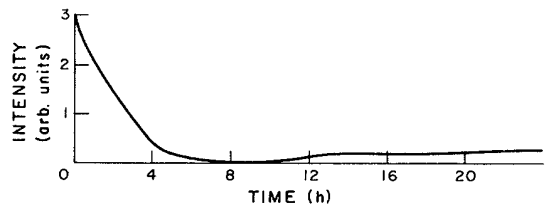

FIG. 9. Cell thermal expansion as a function of time for the 2.1-μm film.

D. Film preparation

The binary liquid mixture used in this study is 2,6-dimethylpyridine (lutidine) and water. It has a lower critical point at about 34 °C which means the mixture is in the

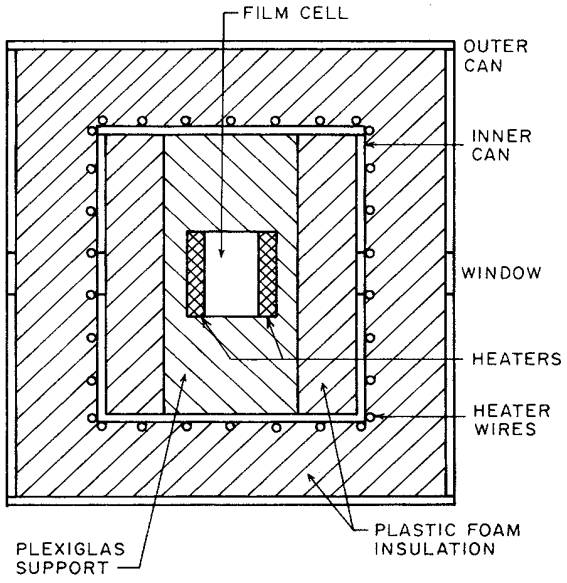

FIG. 10. The temperature-controlled chamber.

one-phase region at room temperature. Thus, a homogeneous stock solution of the mixture can be prepared from which small samples can be drawn to fill the cell as needed. The two liquids have an appreciable refractive index mismatch, the value for water being 1.33 and for lutidine 1.50. This produces strong scattering near the critical point which is a distinct advantage for thin-film studies. Note that the film thicknesses used here, 13.1 μm being the maximum, are much smaller than the photon mean free path in the liquid so that multiple scattering is not a concern.

The lutidine was purchased 99% pure from Eastman Kodak Company and then further purified by distillation. The water was triply distilled and deionized. A stock solution of approximately 155 ml was prepared with a composition of $28.697\pm0.001\%$ lutidine by mass, chosen to agree, within experimental precision, with that used by Schiebner *et al.*[33] This solution was used for the 13.1-, 4.1-, and 2.1-μm-thick films before it was exhausted. The 0.5-μm films were drawn from a 50-ml stock solution prepared with a concentration of $28.701\pm0.001\%$ lutidine by mass.

To clean the cell the several components of the cell first are washed separately in soap and water and rinsed in distilled water that has been filtered through a 0.08-μm Nuclepore filter to remove dust. The separate components are then dried on a laminar flow bench. The cell is assembled with the optical flats spaced a few mm apart. Next the cell is flushed with several ml of the binary liquid mixture which is injected into it with a syringe through a 0.08-μm filter that is attached to a threaded fill port on the cell. The rinse liquid is expelled through a drain port by forcing air through the filter on the fill port. This flushing procedure is repeated several times before the final sample is injected. The sample has a volume of approximately 10 ml. The flats then are pressed against the spacer, trapping the film between them. Finally, Teflon-tipped steel set screws are threaded into the fill and drain ports to seal them.

E. Critical-temperature measurement

We must determine T_c accurately in order to compare the film Rayleigh linewidth data to theory. A method commonly used with bulk samples involves a careful adjustment of the temperature of the liquid mixture until a meniscus appears, marking the transition from the homogeneous to the separated-phase regime. The identification of the phase-separation temperature with T_c presupposes that the system is precisely at the critical composition. This technique does not work for thin films because the surface tension between the optical flats and the liquid phases is sufficiently large to prevent a meniscus from forming. The two phases are essentially trapped between the flats and cannot flow up or down. Nevertheless, a multitude of phase-separation droplets do form when a film is heated into the two-phase region, and they can be observed using a telemicroscope located outside the thermostated chamber.

To determine the phase-separation temperature, the film cell temperature is increased until phase-separation droplets appear. Then the temperature is allowed to drop until the droplets disappear. The temperature is then increased by half the difference between the previous one-phase and two-phase temperatures to see if droplets form. If they do, the temperature is allowed to drop until the droplets disappear again, the temperature increase is halved again, and the procedure is repeated until the droplets do not form. With iteration it is possible to determine the phase-separation temperature, which we identify with T_c, to within ±0.05 mK.

The films respond to temperature changes differently than bulk samples. If phase separation occurs, the droplets are always observed within four hours of the temperature change. If a film is raised a few mK above T_c and phase separation occurs, the phases will recombine within one hour once the temperature has dropped to a few mK below T_c.

To check that a film is truly homogeneous once the droplets have disappeared, it is quenched from the two-phase region to 100 mK below T_c at which point the Rayleigh linewidth is measured. After this cycling and linewidth measurement process, the temperature is again raised into the two-phase region, then lowered to the same few mK below T_c, and the linewidth is measured immediately after the droplets disappear. The two measured linewidths always agree within experimental error.

This distinctive phase-separation behavior of the films provides a test for thermal gradients that is not available in conventional samples. If a film having the critical composition is at a uniform temperature, then the *entire* film should undergo phase separation at T_c. Phase-separation droplets were observed to appear and disappear uniformly across the full extent of our films. This is the basis for our claim that thermal gradients have been reduced below 0.1 mK across the plane of the films.

We emphasize that our method of determining T_c for these films depends upon the correctness of equating it to the phase-separation temperature. Since we have no independent means of checking the film composition, the best we can do is to make the identification and then look for consistency, or the lack of it, when the experimental linewidth dependence on $k\xi$ is compared with theory.

F. Critical-temperature drift

Drifts in the critical temperature with time have been observed in binary liquid mixtures[21,30] but in our case these drifts have in addition a marked dependence on film thickness. In this paper we report measurements on four films, of thicknesses 13.1, 4.1, 2.1, and 0.5 μm.

In the 13.1-μm film we measured an average T_c drift rate of 0.08 mK/day over its 66-day lifetime.

The 4.1-μm film gives the most complete picture of the critical-temperature behavior as a function of time. T_c was measured over the 73-day lifetime of the film and the measured values are plotted in Fig. 11. When the film was two days old the drift rate was 2.3 mK/day. Over the last 25 days of the film's life the drift rate was 0.20 mK/day, during which period we made all the Rayleigh linewidth measurements on it.

In one 2-μm film the T_c drift rate was 3.0 mK/day

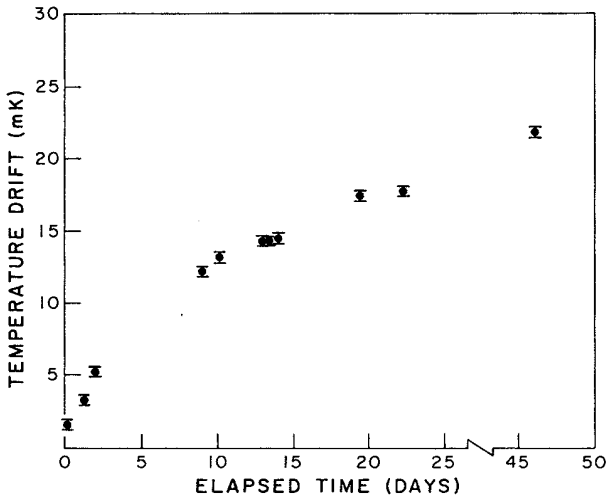

FIG. 11. Drift in critical temperature of the 4.1-μm film as a function of time. Absolute temperature at the origin of the plot is 34.0140°C.

when the film was seven days old, 1.5 mK/day after 17 days, 1.0 mK after 21 days, and 0.5 mK after 25 days. No Rayleigh linewidth data were taken on this particular film. In the 2.1-μm film that was used for linewidth measurements, a drift of 0.4 mK/day was seen after 34 days.

The 0.5-μm film showed a dramatic drift. Eight days after the film was formed the drift rate was 80 mK/day. This slowed to 0.6 mK/day after 35 days.

There are two trends in these drift rates. First, the rate increases with decreasing film thickness. Second, for a given film the rate decreases as the age of the film increases. Sorenson[30] observed a fairly constant drift of 0.05 mK/day in the critical temperature of a bulk sample of methanol and cyclohexane over a nine-month period. He ascribed this to a drift in the thermistor resistance at constant temperature. While this value is comparable to the drift seen in the 13.1-μm film, the time and thickness dependence of the T_c drift rate in our films cannot be explained by invoking a constant thermistor resistance drift rate or even a time-dependent resistance drift rate.

One possible explanation of our observations is that the lutidine interacts chemically with the fused-silica optical flats and the T_c shift is an impurity effect. Although we have no independent support for this hypothesis, it is consistent with the general observation that the *initial* drift rate of the critical temperature increases with decreasing film thickness, and subsequently the drift rate falls to a lower value after conditions approximating a steady state are reached.

Quite apart from considerations of its cause, the T_c drift will introduce a large error in the value of $T-T_c$ unless it is included in the analysis. The linewidth data, except for those from the 0.5-μm film, were taken once the drift rate dropped to a constant value on the order of 0.2 mK/day. All temperatures T are adjusted so that the differences $T-T_c$ reflect the actual value of T_c at the time when the linewidths were measured.

IV. EXPERIMENTAL ANALYSIS AND RESULTS

A. Rayleigh linewidth analysis

As discussed earlier, the Rayleigh linewidth behavior in thin critical fluid films may differ from that in conventional critical fluid samples. In addition, the comparison of measured linewidths to the theoretical prediction, even for conventional samples, requires the folding in of several other experimental factors such as the temperature, the shear viscosity, the correlation length and the relevant wave number. To serve as a check against the possibility that a combination of systematic experimental errors might affect this comparison, we analyzed our data by assuming that they are correctly described by the infinite-volume (3D) theoretical description. This description should at least be appropriate for the films far from the critical point where $\xi \ll s/2$, with $\Lambda \ll s$, and where the presence of systematic errors would be revealed by discrepancies between the film data and theory. Should we find agreement between experiment and theory under these conditions, then we would be prepared to argue that experimentally significant departures of our data from the 3D theory in the $\xi \geq s/2$, $\Lambda \geq s$ regime reflect finite-size changes.

To compare experiment to theory we adopt the standard method for displaying the Rayleigh linewidth[1] Γ. First, Eq. (1) is solved for $\Omega(k\xi)/k\xi$,

$$\Gamma^* = \Omega(k\xi)/k\xi \ , \tag{7}$$

where the *reduced* Rayleigh linewidth Γ^* is defined as

$$\Gamma^* \equiv 6\pi\eta(\xi)\Gamma/Rk_BTk^3 \ . \tag{8}$$

Thus Γ^* is only a function of the product $k\xi$, and a plot of Γ^* vs $k\xi$ should reproduce the theoretical curve $F(k\xi) \equiv \Omega(k\xi)/k\xi$ without adjustable parameters.

The lowest-order Kawasaki function,[6,7] including the higher-order corrections given by Oxtoby and Gelbart,[34] is used to represent $\Omega(k\xi)$. We assume that noncritical background contributions to the scattering are negligible. The fluctuation wave number $k = k_{sc}$ is given by

$$k = \frac{4\pi}{\lambda} \sin\left[\frac{\theta}{2}\right] , \tag{9}$$

where λ is the laser wavelength and θ is the scattering angle in air, 60°±1° for all measurements reported here. The scattering geometry shown in Fig. 1 guarantees that the wave vector $\vec{k}$ lies in the plane of the film. However, we can vary the magnitude of $\vec{k}$ by operating the argon-ion laser at either 457.9, 488.0, or 514.5 nm. This corresponds to a 12% range in k which proves sufficient to enable determination of the dynamic critical exponent z. The correlation length is calculated from the appropriate temperature scaling relation, using $\nu = 0.63$ (Ref. 35) and the value for the amplitude $\xi_0 = 2.0$ Å.[36] The temperature and the critical temperature are measured and their difference is corrected for the drift in T_c. We use the value of the shear viscosity for 2,6-lutidine+water measured near the critical point by Gulari *et al.*[36] and the value for R of 1.020±0.028 reported by Burstyn and Sengers.[2]

Γ is extracted from measurements of the time autocorrelation function of the scattered light. The autocorrelation function is fit to the form

$$C(t)=B+A\exp[-K_1t+(K_2/2)t^2+(K_3/6)t^3]\,, \quad (10)$$

where t is time, B is the background, A is the amplitude, and K_i is the ith cumulant. B is determined by the average count in the last eight channels of the correlator which are delayed 64 sample times beyond the previous channel. A derivation of the heterodyne autocorrelation function[26] shows that B also is found from the total number of photocounts registered by the digital correlator. When the values of B determined in these two ways differ by more than one standard deviation, that autocorrelation function is discarded as unreliable. Once B is found, A and the K_i are determined from a linear least-squares fit to $\ln[C(t)-B]$.

In a careful experiment on a bulk system, Burstyn and Sengers[2] have shown that the autocorrelation function of the Rayleigh scattered light can be represented by an exponential decay linear in t ($K_2=K_3=0$) within the experimental precision of their data for temperatures more than 20 mK away from T_c. Thus K_2 and K_3 are expected to be negligible outside of that range and the Rayleigh linewidth is taken to be $\Gamma=K_1$. Within 20 mK of T_c they found small deviations from exponential decay. In this case, the definition of Γ is unchanged since K_1 represents the *initial* decay of the autocorrelation function. The measure of nonexponentiality is taken to be $Q=K_2/K_1^2$. The value of Q is always small in bulk systems and consistent with zero, within experimental error, for temperatures more than 20 mK away from T_c. However, it is possible that the thin films introduce some nonexponentiality into the autocorrelation function. Therefore, Q will be a parameter of interest. We determine Q from the least-squares result for K_1 and K_2 when Eq. (10) is fit to all 64 channels in the autocorrelation function.

Each of our Γ^* values was derived by taking the average of nominally ten values of Γ extracted from autocorrelation functions measured at fixed T and k. Each autocorrelation function was accumulated for a time such that the estimated error in the fitted value of Γ is about 2%. A typical autocorrelation function with its fitted exponential decay curve is shown in Fig. 12.

Finally, the dynamic scaling exponential z defined in Eq. (3) can be determined by measuring Γ at constant temperature and scattering angle for two different wavelengths. If Γ_1 and Γ_2 are the linewidths measured for λ_1 and λ_2, respectively (λ_1 and λ_2 can be selected from 457.9, 488.0, and 514.5 nm),

$$\Gamma_1/\Gamma_2=(\lambda_2/\lambda_1)^z\,, \quad (11)$$

$$z=\frac{\ln(\Gamma_1/\Gamma_2)}{\ln(\lambda_2/\lambda_1)}\,. \quad (12)$$

B. Rayleigh linewidth results

In this section we report the results of Rayleigh linewidth measurements on four films of thickness 13.1, 4.1, 2.1, and 0.5 μm. All thicknesses have an uncertainty of ±0.1 μm. The data from the three thickest films were reported previously.[15]

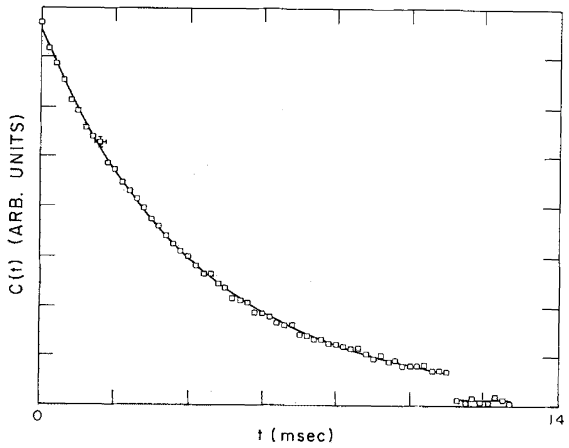

FIG. 12. A fitted heterodyne autocorrelation function for the 4.1-μm film. Last eight channels are delayed by 64 sample times.

1. 13.1-μm film

The reduced Rayleigh linewidth results for the 13.1-μm film are plotted versus $k\xi$ in Fig. 13. The solid line is the universal scaling function appropriate for bulk systems. As can be seen, the agreement between experiment and theory is very good. The value of the reduced χ^2 for the fit is 1.0. The exponent z is calculated using the data closest to T_c. Here, $T_c-T=0.3\pm0.1$ mK and linewidths were measured at 514.5, 488.0, and 457.9 nm. We find $z=3.14\pm0.04$, where the uncertainty is the standard deviation of the individual determinations of z and contains no estimate of systematic errors.

At 13.1 μm, the regime defined by $\xi>s/2$ corresponds to $k\xi=80$ at $\lambda=5.14.5$ nm. We determined one Γ^* value

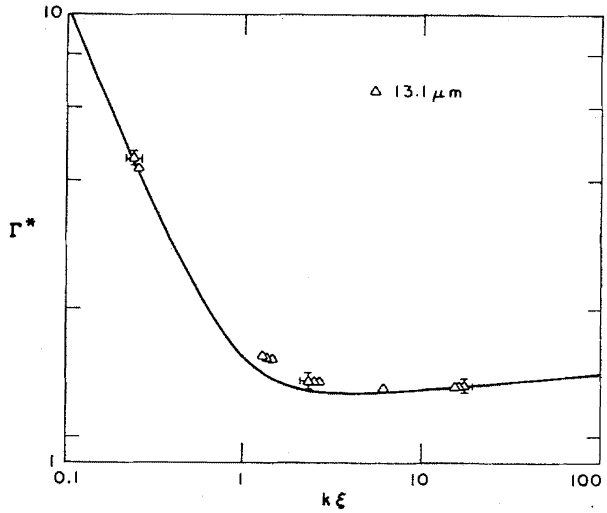

FIG. 13. Reduced Rayleigh linewidths for the 13.1-μm film. In this, and the succeeding data plots, the solid curve is the theoretical prediction for a critical fluid in the large-volume limit. No adjustable parameters are used (from Ref. 15).

at $k\xi > 80$ which was in good agreement with the 3D prediction at the presumed value of $k\xi$. However, the error in ξ is so large for this point that its location on the $k\xi$ axis is problematical and it is not included in Fig. 13. With an operating wavelength of 514.5 nm $\Lambda \simeq s/25$, so that the fluctuation wavelength probed is significantly smaller than the film thickness.

The value of the nonexponentiality factor Q is typically 0.05 for all autocorrelation functions taken on this film. All Q values are within two standard deviations of zero and most lie within one. Q does not increase for $T_c - T < 20$ mK, but this is not surprising given the method of analysis we used. This film was observed over a 66-day period.

2. 4.1-μm film

The reduced linewidths are plotted in Fig. 14 and the agreement between theory and the data is good. The value of the reduced χ^2 is 0.1.

With $s = 4.1$ μm and $\Lambda \simeq 0.5$ μm we have $\Lambda \simeq s/8$, still almost an order of magnitude smaller than the film thickness. The boundary of the $\xi \geq s/2$ regime is defined by $\xi \simeq 2.0$ μm. This corresponds to $T_c - T = 0.13$ mK and $k\xi = 25$. There is only one datum in this zone. It falls somewhat below the theoretical curve but the same discrepancy is found in the linewidth data from other 3D binary liquid systems[34] when $k\xi \gg 1$. All data were taken at 514.5 nm so z was not determined. The values of Q are again small, typically 0.04, and for the most part, consistent with the expected value of zero. This film lasted 73 days without observable changes in composition due to leakage from the surrounding fluid reservoir.

3. 2.1-μm film

The 2.1-μm film is the first with a significant set of data with $\xi > s/2$; $\xi = 1.0$ μm corresponds to $T_c - T = 0.4$ mK and $k\xi = 13$ at 514.5 nm. There are 14 points with $k\xi > 13$. As can be seen from Fig. 15, all the reduced

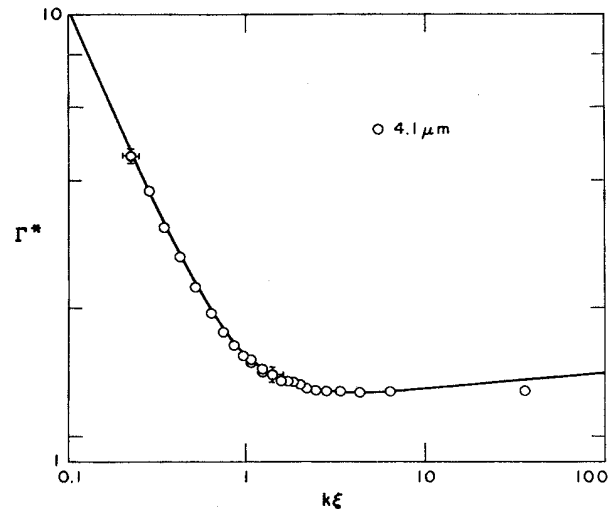

FIG. 14. Reduced Rayleigh linewidths for the 4.1-μm film (from Ref. 15).

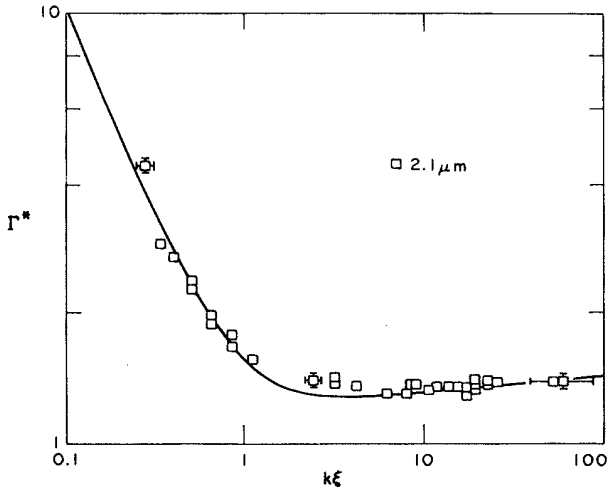

FIG. 15. Reduced Rayleigh linewidths for the 2.1-μm film (from Ref. 15).

Rayleigh linewidth data agree well with the 3D theory. The sampling length $\Lambda \simeq s/4$ for this film. The reduced χ^2 for all the points is 0.7. For the four temperatures for which $\xi > s/2$ in this film, we find $z = 3.11 \pm 0.06$ which agrees with both the 3D RG prediction and the measurement of Burstyn and Sengers.[2] The values of Q are typically 0.1 or 0.2 with standard deviations from 0.03 to 0.04. The Q values are not consistent with $Q = 0$. This film lasted only 40 days, after which the exchange of fluid between the film and the surrounding reservoir became apparent.

4. 0.5-μm film

The reduced linewidth data for the 0.5-μm film are plotted in Fig. 16. For this film, the condition $\Lambda \simeq s$ is satisfied. The data are assembled into three distinct sets distinguished by differences in the film critical-

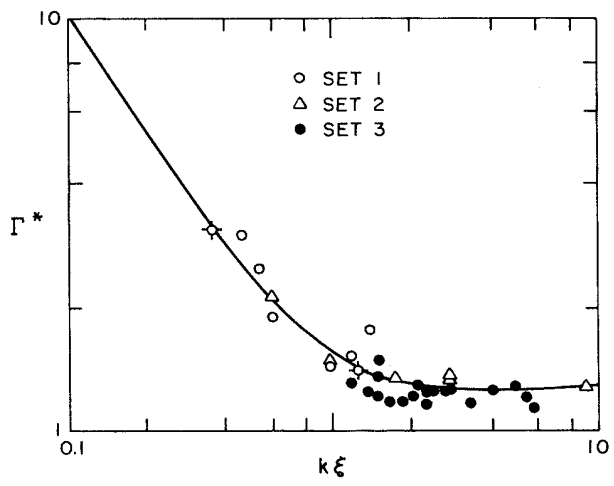

FIG. 16. Reduced Rayleigh linewidths for the 0.5-μm film. Significance of the three distinct data sets is discussed in the text.

temperature drift rate at the times the measurements were made. The condition $\xi \geq 0.25\ \mu$m corresponds to $T_c - T \leq 3.7$ mK and $k\xi \geq 3$ for $\lambda = 514.5$ nm. There are no set-1 points, one set-2 point (two others at $k\xi \simeq 3$), and five set-3 points that lie in this correlation-length regime. The scatter of these Γ^* values is somewhat larger than for the thicker films since the signal level was significantly weaker. The values of the reduced χ^2 for these plots are 4.0, 0.6, and 3.9, for sets 1, 2, and 3, respectively. A number of the set-3 points fall well below the theoretical curve. At first it was suspected that laser heating was producing temperature gradients in the scattering volume and the accompanying convective flow coupled to the order-parameter fluctuations to yield the anomalously small reduced linewidths. However, various tests of this conjecture revealed no statistically significant dependence of the linewidths upon incident laser power. The parameter Q varies between 0.2 and 0.4, with standard deviations ranging from 0.02 to 0.05. There is significant scatter in Q for this film, however, with several values as low as 0.01.

Unlike the thicker films, T_c for the 0.5-μm film could not be determined by measuring the phase-separation temperature. As we argue below, this film behaved as if it were approaching a 3D binary liquid critical point until T got very close to T_c ($T_c - T \simeq 2$ mK). At this point the system seemed to head toward a different transition, probably of first order. Thus T_c was not experimentally accessible and it had to be determined indirectly.

We used the following strategem to find T_c. After being formed, the film was placed in the thermostated chamber and the temperature raised until light scattering could be seen when the path of the incident light through the film was viewed in a telescope. This indicates that the temperature is sufficiently close to T_c that critical fluctuations are present. The temperature and the Rayleigh linewidth were measured and the effective value of $T_c - T$ was determined by fitting this linewidth value to the 3D theoretical curve. The assumption implicit in this approach is that the film is approaching a typical binary liquid critical point. To test this assumption, the linewidth was remeasured after the temperature was increased to a point that should halve the previous fitted value of $T_c - T$. The effective value of $T_c - T$ was determined from this linewidth and found to be in good agreement with that extrapolated from the previous measurement.

We interpret this agreement as evidence that for these temperatures the film is a 3D binary liquid critical system with an effective critical temperature T_c. The reduced linewidth data appearing in Fig. 16 are plotted using this approach. Since the drift rate of the effective T_c determined in this way differs for the three data sets, their separate identities are maintained in the plot.

When the temperature was increased to within 2 mK of the fitted T_c, the autocorrelation signal decreased in intensity, signaling the suppression of critical fluctuations. The scattered intensity and the fluctuation lifetime both decreased monotonically as T was raised above T_c. Phase separation did not occur until the temperature was raised about 150 mK above the fitted T_c, at which point the Rayleigh scattering signal was undetectable. Finally, we also observed that in contrast to the behavior of the thicker films, once the phases separated, the temperature had to be decreased until it was roughly 150 mK *below* T_c in order for them to remix. Once the single-phase regime was entered, a remeasurement of the Rayleigh linewidth reproduced the earlier measured values at that temperature.

Our interpretation of the 0.5-μm film can be summarized as follows. We are able to achieve an internally consistent description of the Rayleigh linewidth data for temperatures to within 2 mK of an effective critical temperature. Thus, for $T_c - T \geq 2$ mK, the film behaves, from the perspective of our experiment, as if it were approaching a normal binary liquid transition at the effective T_c. In addition, the ability of this film to approach to within 2 mK of the fitted T_c, well into the nonhydrodynamic ($k\xi \geq 1$) region, without the appearance of statistically significant discrepancies between the data and predicted 3D behavior, argues against significant off-loading of the film composition. When $T_c - T$ was reduced somewhat below 2 mK, the system would tend toward another type of transition.

5. *Summary of Rayleigh linewidth results*

Figure 17 consists of a plot of the combined reduced Rayleigh linewidth results against $k\xi$ for the three thicker films. In Fig. 18 we plot the 2.1-μm data and the full set of 0.5-μm results against $k\xi$. We emphasize again that no adjustable parameters were used in the comparison between experiment and the 3D theory for the 13.1-, 4.1-, and 2.1-μm films, and aside from the use of an effective T_c as described in Sec. IV B 4, the Γ^* vs $k\xi$ plot for the 0.5-μm film involves no fitting parameters.

There are a number of features apparent in these results that deserve comment. Although the scattering volume has been reduced by up to 3 orders of magnitude in the film studies, a comparison between Fig. 17 and Fig. 10 of the paper by Swinney and Henry[2] reveals that the Γ^* data for the three thicker films compare favorably, both in terms of scatter and the agreement with theory, to the best of the conventional-sample Rayleigh linewidth data considered by those authors in 1973. Even the scatter of the 0.5-μm-film data and their agreement with theory are

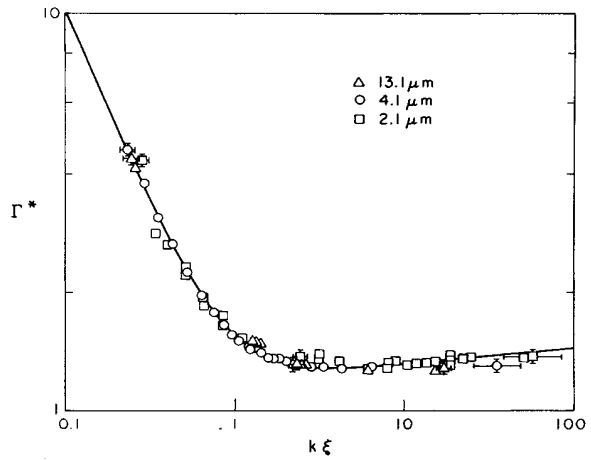

FIG. 17. Combined reduced Rayleigh linewidths for the 13.1-, 4.1-, and 2.1-μm films (from Ref. 15).

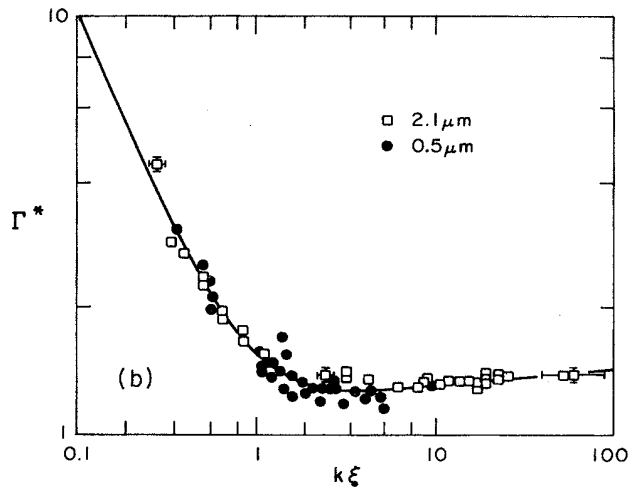

FIG. 18. Reduced Rayleigh linewidths for the 2.1-μm film plotted with the combined set of 0.5-μm film data.

comparable to the better binary-mixture data.[1] Although the high quality of the film data came as a pleasant surprise to us, it can be credited to improvements in temperature control and in the technology of quasielastic light scattering that occurred during the last decade.

As inspected by an experiment probing the fluctuation spectrum at $\Lambda_{max}\simeq 0.51\ \mu$m ($\Lambda_{min}\simeq 0.46\ \mu$m), the three thicker films, and the 0.5-μm film to within 2 mK of its extrapolated critical temperature, behaved dynamically as prototypical critical binary liquids in the large-volume limit. Although a total of 23 Γ^* values were measured under conditions which assured that the continued evolution of order-parameter fluctuations would be suppressed in one spatial dimension, we find no statistically significant indication of a departure from 3D dynamical behavior. This conclusion is particularly strong in the case of the 2.1-μm film, where 14 Γ^* values lie in the $\xi > s/2$ zone and where the reduced χ^2 for the total data set was 0.7.

We determined the dynamic critical exponent z for the 13.1- and 2.1-μm films from the Rayleigh linewidth data, and its wave-number dependence, very near T_c. With an admittedly crude approach we find $z(s=13.1\ \mu\text{m}) = 3.14\pm 0.04$ and $z(s=2.1\ \mu\text{m}) = 3.11\pm 0.06$, compared to the accepted value of $z=3.065$ for a critical binary liquid in 3D.

C. Surface wetting layers

Since one of the components of a binary liquid confined between solid walls will tend to have a greater surface tension relative to the walls than the other, it is energetically favorable for the mixture if that component accumulates along the walls, forming a surface wetting layer. This process has been described by Cahn[13] and by Fisher and de Gennes[10] for a binary liquid in the presence of a single wall, and by Fisher and Nakanishi[12] for a similar system confined between two walls. In both analyses it is assumed that the fluid forming the film or interface is an *open* system which maintains contact with an infinite reservoir of the binary liquid. One consequence of wetting-layer formation which is of direct concern to our work is that the formation of such layers in an open film leads to composition gradients across the film and to *global* shifts in film composition. If a binary fluid film initially formed at the critical composition develops concentration gradients and overall composition shifts with time, the critical Rayleigh scattering will disappear, the lower phase-separation temperature for a mixture such as 2,6-lutidine+water will increase, and the relative volumes of the two phases will change with time.

This picture is altered for our binary liquid films which are closed, having no access, or very restricted access, to the surrounding reservoir of fluid when the cell is properly sealed. Without the possibility of material exchange between film and reservoir, and for chemically inert walls, the overall composition of the film is fixed and entropy counteracts the tendency for surface wetting layers to form.

We found no evidence for the formation of wetting layers during the several-week lifetimes of our films. Eventually, however, the cell spacer rings failed, sometimes catastrophically, at other times slowly, over a period of weeks. When the failure of the seal occurred slowly, we were able to monitor changes in the film over a period of a few days which provided clear evidence that the film composition was drifting. Specifically, the scattering intensity and the fluctuation lifetime measured at fixed T decrease with time. When phase separation can still be observed, it has a different quality than in the sealed films. In the latter case, the separated droplets are large enough to be resolved as such, even at closest approach to the phase-separation temperature, and the estimated volumes of the two phases are roughly equal. For a film in the process of failure, the droplets appear as tiny points, and the volume of the droplet phase is much smaller than that of the surrounding phase. The phase-separation temperature also shows a sudden increase in excess of its established secular drift.

While it is clear that global composition shifts do occur when the film seal aborts, none of the consequences we have discussed demand the presence of wetting layers for their explanation. The presence of surface layers may be essential to what we observed in the 0.5-μm film within 2 mK of T_c, but we have no evidence either in support of or in opposition to this conjecture.

In summary, our Rayleigh scattering studies on closed binary liquid films have revealed no evidence of wetted-layer formation.

V. DISCUSSION

We have demonstrated the technical feasibility of studying the order-parameter dynamics in thin critical fluid films, using heterodyne photon autocorrelation techniques. While our Rayleigh linewidth measurements covered both the hydrodynamic and nonhydrodynamic regimes in all four films, and they contacted the finite-size regime ($\Lambda\simeq s$ and $\xi > s/2$) in the 0.5-μm film these studies

are incomplete. It is important that we extend the measurements to forward angles to enable coverage of the $\Lambda > s$ regime for films as thick as 2 μm whose behavior near T_c seems less complicated than is the case for a 0.5-μm film. (For example, $\Lambda \simeq 6$ μm for $\lambda = 514.5$ nm and $\theta = 5°$.) In addition, we must select a different binary mixture, neither of whose components interact chemically with the fused-silica flats of our sample cell. If our conjecture is correct, that the time- and thickness-dependent drifts in T_c we have seen follow from the 2,6-lutidine interacting with the flats, then closed thin films of a chemically inert mixture should have time-independent critical temperatures.

ACKNOWLEDGMENTS

We acknowledge useful discussions with M. Calvo, H. Nakanishi, and A. J. Hurd. We particularly wish to acknowledge a valuable suggestion made by Lise K. Cotter which we incorporated into the design of our sample cell. This research was supported by U. S. Department of Energy Grant No. DE-AC02-82ER13004.

*Present address: Institute for Polymers and Organic Solids, University of California, Santa Barbara, CA 93106.

[1]H. L Swinney and D. L. Henry, Phys. Rev. A 8, 2586 (1973).
[2]H. C. Burstyn and J. V. Sengers, Phys. Rev. A 25, 448 (1982).
[3]H. C. Burstyn, R. F. Chang, and J. V. Sengers, Phys. Rev. Lett. 44, 410 (1980).
[4]H. C. Burstyn, J. V. Sengers, and P. Esfandiari, Phys. Rev. A 22, 282 (1980).
[5]R. F. Chang, H. C. Burstyn, and J. V. Sengers, Phys. Rev. A 19, 866 (1979).
[6]K. Kawasaki, Phys. Lett. 30, 325A (1969).
[7]K. Kawasaki, Ann. Phys. (N.Y.) 61, 1 (1970).
[8]E. D. Siggia, B. I. Halperin, and P. C. Hohenberg, Phys. Rev. B 13, 2110 (1976).
[9]M. E. Fisher, J. Vac. Sci. Technol. 10, 665 (1973).
[10]M. E. Fisher and P. G. de Gennes, C. R. Acad. Sci. Paris, Ser. B 287, 207 (1978).
[11]M. E. Fisher and H. Au-Yang, Physica 101A, 255 (1980).
[12]M. E. Fisher and H. Nakanishi, J. Chem. Phys. 75, 5857 (1981).
[13]J. W. Cahn, J. Chem. Phys. 66, 3667 (1977).
[14]M. R. Moldover and R. W. Gammon (unpublished).
[15]S. A. Casalnuovo, R. C. Mockler, and W. J. O'Sullivan, Phys. Rev. Lett. 98, 939 (1982).
[16]P. C. Hohenberg and B. I. Halperin, Rev. Mod. Phys. 49, 435 (1977).
[17]B. I. Halperin and P. C. Hohenberg, Phys. Rev. Lett. 19, 700 (1967).
[18]B. I. Halperin and P. C. Hohenberg, Phys. Rev. 177, 952 (1969).
[19]B. I. Halperin (private communication).
[20]D. Gutkowicz-Kusin and I. Procaccia, Phys. Rev. A 27, 2585 (1983).
[21]C. Franck and S. E. Schnatterly, Phys. Rev. Lett. 48, 763 (1982).
[22]D. Beysens and S. Leibler, J. Phys. (Paris) Lett. 43, L133 (1981).
[23]W. Goldburg (private communication).
[24]O'D. Kwon, D. Beaglehole, W. W. Webb, B. Widom, J. W. Schmidt, J. W. Cahn, M. R. Moldover, and B. Stephenson, Phys. Rev. Lett. 48, 185 (1982).
[25]S. A. Casalnuovo, Ph.D. thesis, University of Colorado, Boulder, Colorado, 1982 (unpublished).
[26]J. Lastovka, Ph.D. thesis, Massachusetts Institute of Technology, Cambridge, Massachusetts, 1967 (unpublished).
[27]B. J. Berne and R. Pecora, *Dynamic Light Scattering* (Wiley, New York, 1976).
[28]A. J. Hurd, Ph.D. thesis, University of Colorado, Boulder, Colorado, 1981 (unpublished).
[29]M. A. Handschy (private communication).
[30]C. M. Sorensen, Ph.D. thesis, University of Colorado, Boulder, Colorado, 1976 (unpublished).
[31]M. A. Handschy, J. Phys. E 13, 998 (1980).
[32]C. M. Sorensen, R. C. Mockler, and W. J. O'Sullivan, Phys. Rev. Lett. 40, 777 (1976).
[33]B. A. Scheibner, M. R. Meadows, R. C. Mockler, and W. J. O'Sullivan, Phys. Rev. Lett. 43, 590 (1979).
[34]D. W. Oxtoby and W. M. Gelbart, J. Chem. Phys. 61, 2957 (1974).
[35]J. C. Le Guillou and J. Zinn-Justin, Phys. Rev. Lett. 39, 95 (1977).
[36]E. Gulari, A. F. Collings, R. L. Schmidt, and C. J. Pings, J. Chem. Phys. 56, 6169 (1972).